



Microscopic description of intermediate mixed state in superconductors between the first and second types

Vyacheslav D. Neverov ^{1,2} Alexander E. Lukyanov ^{1,2} Andrey V. Krasavin ^{1,2}
Arkady A. Shanenko ^{2,4,*} Mihail D. Croitoru ^{2,3} and Alexei Vagov^{2,4}

¹*National Research Nuclear University MEPhI, Moscow 115409, Russian Federation*

²*HSE University, Moscow 101000, Russian Federation*

³*Departamento de Física, Universidade Federal de Pernambuco, 50740-560 Recife-PE, Brazil*

⁴*Moscow Center for Advanced Studies, Kulakova str. 20, Moscow 123592, Russian Federation*



(Received 30 April 2024; revised 10 July 2024; accepted 12 July 2024; published 2 August 2024)

It has long been known that superconductors in the crossover between superconductivity types I and II exhibit an intermediate mixed state (IMS) with exotic flux configurations such as vortex clusters and chains. Achieving a comprehensive microscopic description of the vortex configurations within this intertype region has proven elusive until now due to the large computational demands involved. We have addressed this long-standing problem by presenting microscopic calculations of the IMS configurations. Our calculations, performed at zero temperature, reveal key features of the IMS, including the formation of vortex clusters and the multivortex nature of interactions between vortices. The obtained boundaries of the IT domain reproduce existing experimental observations remarkably well. Also, the results match earlier findings obtained using the perturbation theory in the vicinity of the critical temperature.

DOI: [10.1103/PhysRevB.110.054502](https://doi.org/10.1103/PhysRevB.110.054502)

I. INTRODUCTION

The interaction between magnetic fields and superconductors unveils a diverse manifold of complex phenomena. Superconductors, distinguished by their response to magnetic fields, are traditionally divided into two conventional types based on how an applied magnetic field interacts with the superconducting condensate [1–3]. In type I, the magnetic field is entirely expelled, while in type II, the magnetic field can partially penetrate the condensate, leading to the formation of a mixed state. In this mixed state, Abrikosov vortices, each carrying a single quantum of magnetic flux, repel each other and arrange into a periodic lattice [4]. The distinction between these two types is based on the dimensionless parameter κ , which is defined as the ratio of the magnetic London penetration depth λ_L to the Ginzburg-Landau (GL) coherence length ξ_{GL} [1–3]. According to the GL theory [5], type-I superconductivity occurs when $\kappa_{GL} < \kappa_0$, whereas type-II superconductivity takes place at $\kappa_{GL} > \kappa_0$, where $\kappa_0 = 1/\sqrt{2}$ is the critical value at which the transition between these conventional superconductivity types occurs.

Notably, extensive investigations into the magnetic responses of certain materials with $\kappa_{GL} \approx 1$ have unveiled superconductors that defy conventional dual classification [6–26]. Experimental findings have shed light on the existence of an intermediate mixed state (IMS) within these crossover materials [7–10,17]. In this unique state, the magnetic field penetrates the superconductor while giving rise to a diverse array of spatial configurations, including Meissner domains

coexisting with vortex lattice islands, vortex clusters, and chains, among others. Initially termed as type II/1 [17], these materials were also referred to as intertype (IT) superconductors [27–30].

Previous theoretical studies linked the observed IMS flux patterns to the existence of spatially nonmonotonic interactions between vortices, which are attractive at long and repulsive at short distances (see, e.g., the review in Ref. [17]). These interactions induce an instability of the Abrikosov lattice, resulting in its fragmentation into vortex clusters, chains, and other structures. Recent studies [31,32] have emphasized that the physics governing the IT regime cannot be fully explained by pairwise vortex interactions alone, as the many-vortex interactions play a crucial role in this regime.

For temperatures below the critical temperature T_c , the IMS state is observed in materials in a finite interval of κ_{GL} values close to κ_0 , which increases as the temperature T decreases. The origin of IT superconductivity is closely linked to the critical Bogomolnyi (\mathcal{B}) point (κ_0, T_c) of the BCS theory [33,34]. This point demarcates the boundary between superconductivity types I and II as the temperature approaches T_c , and is characterized by a self-dual, infinitely degenerate IMS state appearing at the thermodynamic critical field. This state encompasses various conceivable flux-condensate configurations. Deviations from this point lift the degeneracy, leading to the formation of a finite IT domain with exotic flux configurations. This mechanism is universal and applies to both single- and multiband superconductors [27].

Despite the long-standing recognition of the IT regime as a fundamental property that significantly broadens the standard dual classification of superconductivity types, even in conventional superconductors, theoretical investigations

*Contact author: ashanenko@hse.ru

into IT physics have lagged behind. This lack of progress has been attributed to the necessity for calculations to go beyond GL theory, which proves inadequate in describing the IT regime even in proximity to T_c . As a consequence, until recently only the boundaries of the IT domain in the $\kappa_{\text{GL}}\text{-}T$ plane have been calculated [27,35–40]. A theoretical analysis of IMS configurations has only recently been attempted. In particular, it has been conducted using the perturbation expansion of the microscopic BCS theory with respect to the proximity to the \mathcal{B} point, where leading corrections to the GL theory are included [28]. This approach enables the description of arbitrary IMS flux-condensate patterns near T_c in conventional single-band superconductors, yielding the phase diagram of the IT domain. Notice that at $T \gtrsim 0.6T_c$ the perturbative expansion [27] has accurately reproduced the boundaries of the IT domain, extracted from experimental results and a stability analysis of a vortex lattice within the microscopic theory.

However, the results based on the perturbation expansion are applicable only at high temperatures. Achieving a comprehensive microscopic description of the IMS that is valid also at lower temperatures is extremely demanding due to the highly inhomogeneous and irregular nature of this state. This work solves this long-standing problem and presents microscopic theory calculations for few-vortex states in the entire IT domain in a conventional single-band superconductor at $T = 0$. The calculations demonstrate that the main characteristics of the IT domain at lower temperatures remain qualitatively similar to those close to T_c . The obtained zero-temperature boundaries of the IT domain agree well with the universal material-independent experimental measurements for a broad class of conventional superconductors.

II. MODEL

The calculations are performed using a standard attractive Hubbard model described by the Hamiltonian

$$\hat{\mathcal{H}} = \sum_{ij\sigma} t_{ij} \hat{c}_{i\sigma}^\dagger \hat{c}_{j\sigma} - g \sum_{i,\sigma} \hat{n}_{i\uparrow} \hat{n}_{i\downarrow}, \quad (1)$$

where \hat{c}_i is the electron operator at site i of the lattice, σ is the electron spin, t_{ij} is the hopping amplitude between sites i and j , which is nonzero $t_{ij} = -t$ only for the nearest neighbors, and $g > 0$ is the BCS coupling constant. The magnetic field is taken into account through the Peierls substitution, which modifies the hopping integral as $t_{ij} \rightarrow t_{ij} \exp[-i \frac{e}{\hbar c} \int_{\mathbf{r}_i}^{\mathbf{r}_j} \mathbf{A}(\mathbf{r}) \cdot d\mathbf{r}]$, where $\mathbf{A}(\mathbf{r})$ is the vector potential of the field $\mathbf{B} = \nabla \times \mathbf{A}$.

The superconductivity is described within the mean-field approximation, which yields the Bogoliubov–de Gennes (BdG) equations [41,42] for the particlelike and holelike components of the wave function u_i and v_j as

$$\begin{aligned} \sum_j [t_{ij} + (U_i - \mu)\delta_{ij}]u_j + \Delta_i v_i &= E u_i, \\ -\sum_j [t_{ij}^* + (U_i - \mu)\delta_{ij}]v_j + \Delta_i^* u_i &= E v_i, \end{aligned} \quad (2)$$

where μ is the chemical potential, and the site-dependent gap function (order parameter) Δ_i and Hartree-Fock potential U_i

obey the self-consistency equations

$$\Delta_i = g \langle \hat{c}_{i\uparrow} \hat{c}_{i\downarrow} \rangle, \quad U_i = -\frac{g}{2} \sum_{\sigma} n_{i\sigma}, \quad N_e = \sum_{i\sigma} n_{i\sigma}, \quad (3)$$

where $n_{i\sigma} = \langle \hat{c}_{i\sigma}^\dagger \hat{c}_{i\sigma} \rangle$ with $\langle \cdots \rangle$ denoting statistical averaging. These equations are solved together with the Ampère-Maxwell equation for the magnetic field, transformed into the Biot-Savart equation

$$\mathbf{A}_{\text{ind}} = \int_V \frac{\mathbf{j}(\mathbf{r}', \mathbf{A}_0, \mathbf{A}_{\text{ind}}) dV'}{|\mathbf{r} - \mathbf{r}'|}. \quad (4)$$

Here, the total vector potential is represented as $\mathbf{A} = \mathbf{A}_0 + \mathbf{A}_{\text{ind}}$, where $\nabla \times \mathbf{A}_0 = \mathbf{B}_0$ is a uniform externally applied field and \mathbf{A}_{ind} is generated by the emerging superconducting current. The latter explicitly depends on the vector potential through the Peierls factors in the hopping integrals. Solving the BdG equations self-consistently with respect to the gap, the Hartree-Fock potential, and the magnetic field is rather nontrivial because of the convergence problems. To obtain the solution we employ the recently developed algorithm [41], which involves two consistency circles and an explicit solution of the Biot-Savart equation.

The solution is obtained for a three-dimensional (3D) sample, which is $N \times N$ along the x and y axes and is infinite along the z axis. All lengths in the problem are expressed in units of the lattice constant a , while the energy unit of the problem is t . The magnetic field has only a z component $\mathbf{B} = (0, 0, B)$, so that the model is essentially 2D. Notice that the integral in the Eq. (4) is still 3D.

In the calculations, the size of the sample is chosen as $N = 31$, which is much larger than the characteristic lengths of the superconducting state. Hopping elements t_{ij} are zero outside the sample, which can be taken into account by using the boundary conditions $u = 0, v = 0$ for the sites next to the sample. We assume the average filling of $n = 0.25$ electrons per 2D unit cell, whereas 1D density n_z along the z axis is absorbed in constants of the BdG and Ampère-Maxwell equations.

III. RESULTS

We present the calculations for the mixed state with two, three, and four vortices. This is sufficient to demonstrate the appearance of the IT regime and investigate the essential characteristics of its IMS, in particular, the many-body aspect of the vortex interactions. At the same time, the calculations in this case can be done for the small system size of $N = 31$ taking a reasonably short time.

Results of the calculations are illustrated in Fig. 1, which plots the spatial distribution of the magnetic field for the mixed states with two, three, and four vortices, obtained for selected values of the coupling constant in the interval $2.0 < g < 3.6$. The figure demonstrates an evolution of the mixed superconducting state between type-II and type-I regimes. The left panels, obtained at $g = 3.6$, show well-separated single quantum Abrikosov vortices, typical for type II. Notice that vortices are repelled from the boundaries, which keep them from moving away. The boundary effects make two vortices in Fig. 1(a) align along a square diagonal. Three vortices in Fig. 1(b) form an equidistant triangle, which denotes

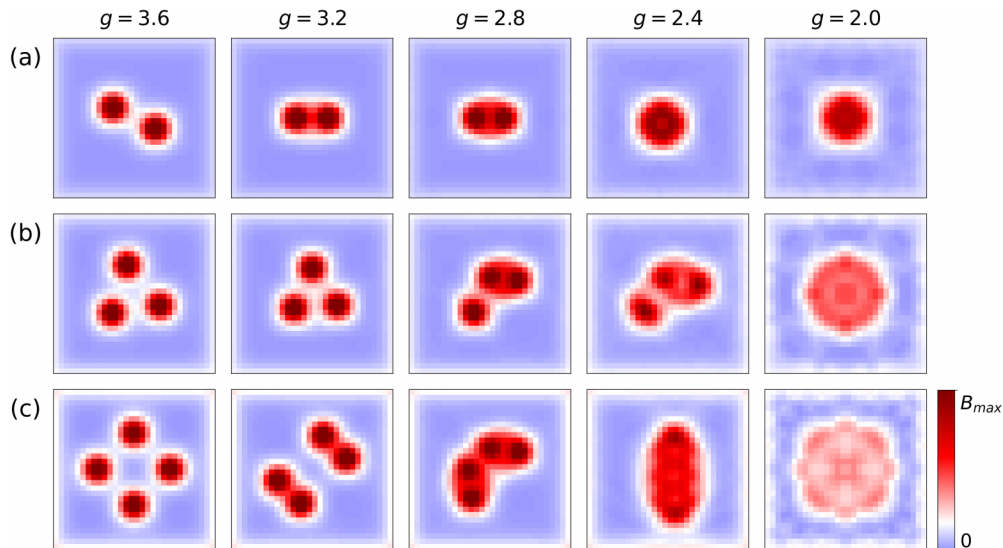


FIG. 1. Spatial profile of the magnetic field inside the sample calculated for configurations with (a) two, (b) three, and (c) four vortices for various values of the superconducting coupling constant g . The value of the external magnetic field is $H = n\Phi_0/S$, where $S = N \times N$ is the sample area, Φ_0 is the flux quantum, and (a) $n = 2$, (b) $n = 3$, (c) $n = 4$.

a standard Abrikosov lattice. Four vortices in Fig. 1(c) are arranged in a square, following the sample geometry.

When g decreases, vortices move closer one to another. This indicates that their interaction potential becomes non-monotonic with the minimum defining the distance between the vortices. This distance is reduced with decreasing g , until vortices merge into a large multi-quantum vortex, as shown in the right panels of Fig. 1. This merging is the reason for the formation of lamellas in the intermediate state of a type-I superconductor (when keeping the total magnetic flux constant). The crossover regime, demonstrated in the figure, is essentially the IT regime with the IMS. It is important to note that the obtained vortex configurations are very similar to those calculated previously within the perturbation theory [28].

Comparing results for different numbers of vortices in Fig. 1 reveals another feature specific to the IT regime and found previously within the perturbative results [31,32]: an important role of the many-vortex interactions. This follows from the fact that the intervortex distance evolution qualitatively depends on the number of vortices. If the interaction between vortices were a sum of pairwise contributions, the distance between neighboring vortices would not depend on the number of vortices in the cluster so that the latter would preserve its shape with decreasing g . However, Fig. 1 demonstrates that the intervortex distance is smaller in vortex pairs than in larger clusters, and the shape of the clusters depends on both the value of g and on the number of vortices in the cluster.

A remarkable example of the difference between the two- and many-vortex interactions can be found in Fig. 1 for $g = 2.4$. Here, the two-vortex cluster merges into a single two-quantum vortex, indicating that the two-vortex interaction is fully attractive. In contrast, three- and four-vortex clusters do not collapse, meaning that the three- and four-vortex interactions are still repulsive at small separations between vortices. This fact was earlier noted for clusters of few vortices within the perturbation theory [32].

The role of the many-vortex interactions is also manifested in that vortices tend to align themselves in bound pairs inside large vortex clusters. In particular, this is seen for both three- and four-vortex clusters in Fig. 1. This tendency is quantified in Fig. 2, which plots the maximal r_{\max} and minimal r_{\min} distances between vortices in the three-vortex cluster versus g . Here, the position of any vortex is obtained as the corresponding point of the vanishing gap function.

At $g \gtrsim 3$, $r_{\max} = r_{\min}$, which corresponds to the formation of an equidistant triangle [cf. Fig. 1(b) for $g = 3.6$ and 3.2]. However, when g decreases, $r_{\min} \neq r_{\max}$, and the equidistant triangle shape breaks down. Two vortices in the cluster form a closely bound pair whereas the third one is located far from this pair. This asymmetry is another indication that the interaction between three vortices differs from that in the pair.

An increased role of the many-vortex interaction in the IT regime can be explained by estimating the energy of the vortex cluster, which is the sum of the contributions of the magnetic field E_B and the condensate E_Δ . The latter is found as the energy loss due to the absence of the condensate in vortex cores. For a single vortex the latter is estimated as proportional

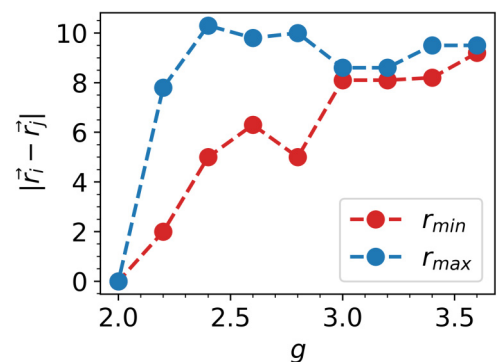


FIG. 2. Minimal r_{\min} and maximal r_{\max} distances between vortices in the three-vortex cluster as a function of g .

to the vortex core area $E_{\Delta} \propto S_1$. When the cores overlap, the energy is defined by the total area,

$$\sum_i S_i - \sum_{i<j} S_i \cap S_j + \sum_{i<j<k} S_i \cap S_j \cap S_k - \dots \quad (5)$$

The first contribution to this sum gives the energy of separated vortices, the second term is the pairwise interaction due to pair overlaps of vortices, the third one is the three-body interaction due to the triple overlaps, etc. Contributions in Eq. (5) have alternating signs. The sign of the pair overlapping is negative, yielding the attractive potential. In contrast, the contribution of the triple overlapping has a positive sign which means an additional repulsive contribution when three vortices are close. This explains why the three-vortex cluster does not collapse even if the pairwise vortex-vortex interaction is fully attractive.

It is important that in the IT regime, where $\lambda \simeq \xi$, the multiple overlapping of vortex cores is significant, and the many-vortex component of the vortex interactions is considerable. In contrast, in type-II superconductors, where $\lambda \gg \xi$, the interaction is mostly defined by the field contribution. The field created by several vortices is additive, $\mathbf{B} = \sum_i \mathbf{B}_i$, and the energy of the magnetic field $E_B \propto \sum_{ij} \mathbf{B}_i \mathbf{B}_j$. It contains interactions for all vortex pairs but does not have three-vortex contributions.

We have seen that when the coupling parameter g varies from 3.6 down to 2, the system evolves along the crossover from type II to type I, passing through the IT superconductivity regime with the IMS formations. Earlier experimental investigations [6–12] (see also Ref. [27]) attributed the IT domain at $T = 0$ to the particular range of the GL parameter $0.6 \lesssim \kappa_{GL} \lesssim 1.2$. It is then instructive to establish a connection between parameters of our microscopic model and κ_{GL} , to see if the IT interval observed in the microscopic calculations corresponds to the IT interval investigated in earlier works.

Although the GL parameter does not enter the microscopic model and thus cannot be controlled directly, one can estimate its value by calculating the zero-temperature superconducting coherence length $\xi(0)$ and the magnetic penetration depth $\lambda(0)$. Notice that the ratio $\lambda(0)/\xi(0)$ does not give the exact value of κ_{GL} . The latter is defined by the ratio of the GL coherence length and the London penetration depth, and therefore should be obtained from the limit $\lambda(T \rightarrow T_c)/\xi(T \rightarrow T_c)$. Nevertheless, as $\lambda(T)$ and $\xi(T)$ are roughly proportional to $(1 - T/T_c)^{1/2}$ [27], one can expect a reasonably good estimate for κ_{GL} extracted from the calculations at $T = 0$.

The values of the $\xi(0)$ and $\lambda(0)$ are extracted from the solution of the microscopic equations for a single vortex shown in Fig. 3, where one sees a spatial profile (radial dependence) of the gap function $\Delta(r)$ and the magnetic field $B(r)$ for the vortex cross section. The characteristic lengths are extracted by fitting these dependencies with exponentially decaying functions.

Obtained $\xi(0)$ and $\lambda(0)$ are shown in Fig. 4(a) as functions of the coupling constant g . $\xi(0)$ is a decreasing function, which is expected, given the standard BCS estimate $\xi(0) \propto \Delta^{-1}$ and the fact that the gap increases with the cou-

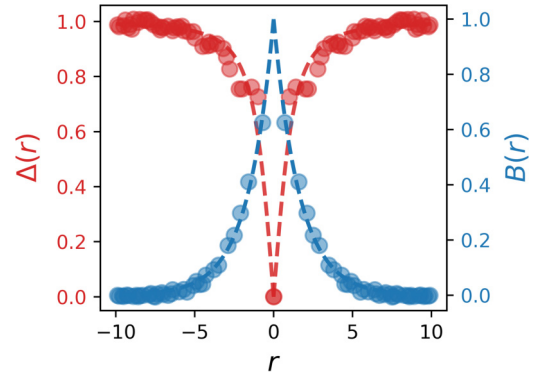


FIG. 3. Radial dependence of the order parameter (red points) and magnetic field (blue points) across a single vortex solution. Connecting dashed lines are drawn as a guide to the eye.

pling. $\lambda(0)$ is also a decreasing function, however, it saturates at large values of g .

The ratio $\kappa(0) = \lambda(0)/\xi(0)$ increases with the coupling, passing through the interval of $\kappa(0) \sim 1$ when $g \sim 2.5$ [see Fig. 4(b)]. This indeed corresponds to the interval when one finds the IT regime with the IMS (see Fig. 1). The insets with the field density plots in Fig. 4(b) give the three-vortex configurations corresponding to the selected values of $\kappa(0)$. The calculations reveal that the IT interval is $0.9 \lesssim \kappa(0) \lesssim 2$. Notice that in order to compare it with the usual definition of the GL parameter κ_{GL} , one needs to

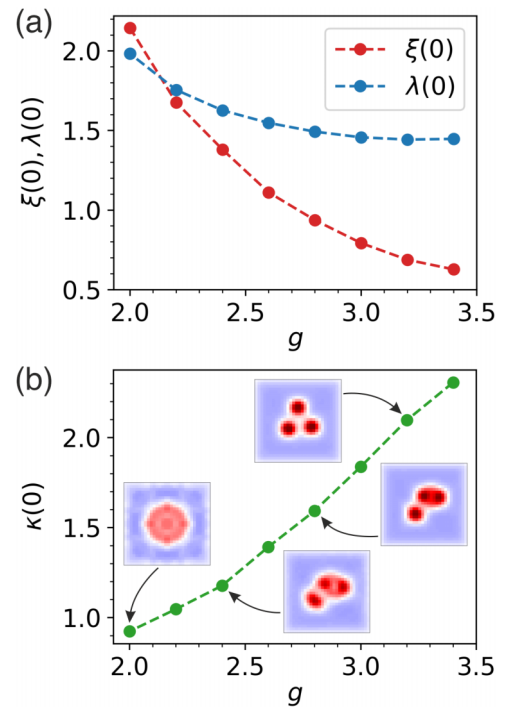


FIG. 4. (a) Condensate coherence length $\xi(0)$ (red) and magnetic penetration length $\lambda(0)$ (blue) are shown as a function of g . (b) The parameter $\kappa(0) = \xi(0)/\lambda(0)$ as a function of g is shown together with the corresponding field distributions from Fig. 1. Dashed lines in both panels are shown as a guide to the eye.

scale it as $\tilde{\kappa}(0) = \kappa(0)/\sqrt{2}$, so that the scaled IT interval is $0.6 \lesssim \tilde{\kappa}(0) \lesssim 1.4$. It is very close to the experimentally reported IT interval at zero temperature [10,27].

IV. CONCLUSIONS

This work presents a microscopic analysis of the IMS in IT superconductors. This analysis is achieved by tracing the evolution of two-, three-, and four-vortex configurations through the entire IT domain by numerically solving the BdG equations for the lattice Hubbard model with an on-site attraction. The solution employs a recently developed approach that is fully self-consistent regarding both the superconducting gap and magnetic field [41]. Notably, this approach does not rely on any prior knowledge of the IMS configuration, which can be arbitrarily complex.

The calculations reveal key features of the IMS configurations at $T = 0$, including the formation of vortex clusters and the many-vortex nature of interactions between vortices. Despite the simplicity of the model, the obtained interval of the IT domain aligns quantitatively remarkably well with existing experimental observations. Moreover, the results confirm earlier findings of the perturbative analysis [27,28,31] for temperatures close to T_c , thus highlighting the universal character of IT superconductivity physics mentioned in Ref. [28]. The microscopic analysis presented

here thus serves as an important milestone in understanding the general phenomenon of IT superconductivity.

Finally, this work is restricted to the mean-field theory analysis and does not take into account fluctuations [43,44] which might be of relevance, especially in the IT regime close to the degeneracy. However, the fact that our results nicely fit experimental data in the entire temperature range (when combining with the perturbation expansion of the mean-field theory), leads to the conclusion that the fluctuations do not play a significant role.

ACKNOWLEDGMENTS

The preparation of the numerical code for solving the governing equations was supported by the Basic Research Program of the HSE University. M.D.C. acknowledges partial support from the UFPE Propeq program (grant Edital Professor Visitante - Edital Propeq No. 05.2018), Recife-PE, Brazil. V.D.N., A.E.L. and A.V.K. acknowledge the Ministry of Science and Higher Education of the Russian Federation (Agreement No. 075-15-2021-1352) for the financial support. The calculations were performed with the support of the MEFPhI Program Priority 2030. A.A.S. and A.V. thank the Russian Science Foundation (Project no. 23-72-30004 [45]) for the support of the analysis of the numerical results for the vortex clustering.

-
- [1] P. G. de Gennes, *Superconductivity of Metals and Alloys* (Benjamin, New York, 1966).
- [2] E. M. Lifshitz and L. P. Pitaevskii, *Statistical Physics, Course of Theoretical Physics Part II* (Pergamon Press, Oxford, UK, 1980), Vol. 9.
- [3] J. B. Ketterson and S. N. Song, *Superconductivity* (Cambridge University Press, Cambridge, UK, 1999).
- [4] A. A. Abrikosov, On the Magnetic properties of superconductors of the second group, *Sov. Phys. JETP* **5**, 1174 (1957).
- [5] L. D. Landau, *Collected Papers* (Pergamon Press, Oxford, UK, 1965).
- [6] H. Träuble and U. Essmann, Die beobachtung magnetischer Strukturen von Supraleitern zweiter art, *Phys. Status Solidi B* **20**, 95 (1967).
- [7] U. Krägeloh, Flux line lattices in the intermediate state of superconductors with Ginzburg-Landau parameters near $1/\sqrt{2}$, *Phys. Lett. A* **28**, 657 (1969).
- [8] U. Essmann, Observation of the mixed state, *Physica* **55**, 83 (1971).
- [9] D. R. Aston, L. W. Dubeck, and F. Rothwarf, "Intermediate mixed" state of type-II superconductors, *Phys. Rev. B* **3**, 2231 (1971).
- [10] J. Auer and H. Ullmaier, Magnetic behavior of type-II superconductors with small Ginzburg-Landau parameters, *Phys. Rev. B* **7**, 136 (1973).
- [11] H. R. Kerchner, D. K. Christen, and S. T. Sekula, Equilibrium properties of the fluxoid lattice in single-crystal niobium. I. Magnetization measurements, *Phys. Rev. B* **21**, 86 (1980).
- [12] H. W. Weber, E. Seidl, M. Botlo, C. Laa, E. Mayerhofer, F. M. Sauerzopf, R. M. Schalk, H. P. Wiesinger, and J. Rammer, Magnetization of low- κ superconductors I the phase transition at H_{c1} , *Physica C* **161**, 272 (1989).
- [13] Y. Wang, R. Lortz, Y. Paderno, V. Filippov, S. Abe, U. Tutsch, and A. Junod, Specific heat and magnetization of a ZrB₁₂ single crystal: Characterization of a type-II/I superconductor, *Phys. Rev. B* **72**, 024548 (2005).
- [14] M. Laver, E. M. Forgan, S. P. Brown, D. Charalambous, D. Fort, C. Bowell, S. Ramos, R. J. Lycett, D. K. Christen, J. Kohlbrecher, C. D. Dewhurst, and R. Cubitt, Spontaneous symmetry-breaking vortex lattice transitions in pure niobium, *Phys. Rev. Lett.* **96**, 167002 (2006).
- [15] M. Laver, C. J. Bowell, E. M. Forgan, A. B. Abrahamsen, D. Fort, C. D. Dewhurst, S. Mühlbauer, D. K. Christen, J. Kohlbrecher, R. Cubitt, and S. Ramos, Structure and degeneracy of vortex lattice domains in pure superconducting niobium: A small-angle neutron scattering study, *Phys. Rev. B* **79**, 014518 (2009).
- [16] S. Mühlbauer, C. Pfeleiderer, P. Böni, M. Laver, E. M. Forgan, D. Fort, U. Keiderling, and G. Behr, Morphology of the superconducting vortex lattice in ultrapure niobium, *Phys. Rev. Lett.* **102**, 136408 (2009).
- [17] E. H. Brandt and M. P. Das, Attractive vortex interaction and the intermediate-mixed state of superconductors, *J. Supercond. Novel Magn.* **24**, 57 (2011).
- [18] A. Pautrat and A. Brûlet, Temperature dependence of clusters with attracting vortices in superconducting niobium studied

- by neutron scattering, *J. Phys.: Condens. Matter* **26**, 232201 (2014).
- [19] J.-Y. Ge, J. Gutierrez, A. Lyashchenko, V. Filipov, J. Li, and V. V. Moshchalkov, Direct visualization of vortex pattern transition in ZrB_{12} with Ginzburg-Landau parameter close to the dual point, *Phys. Rev. B* **90**, 184511 (2014).
- [20] T. Reimann, S. Mühlbauer, M. Schulz, B. Betz, A. Kaestner, V. Pipich, P. Böni, and C. Grünzweig, Visualizing the morphology of vortex lattice domains in a bulk type-II superconductor, *Nat. Commun.* **6**, 8813 (2015).
- [21] J.-Y. Ge, V. N. Gladilin, N. E. Sluchanko, A. Lyashenko, V. B. Filipov, J. O. Indekeu, and V. V. Moshchalkov, Paramagnetic Meissner effect in ZrB_{12} single crystal with non-monotonic vortex-vortex interactions, *New J. Phys.* **19**, 093020 (2017).
- [22] B. Lv, M. Li, J. Chen, Y. Yang, S. Wu, L. Qiao, F. Guan, H. Xing, Q. Tao, G.-H. Cao, and Z.-A. Xu, Type-I superconductivity in noncentrosymmetric NbGe_2 , *Phys. Rev. B* **102**, 064507 (2020).
- [23] P. K. Biswas, F. N. Rybakov, R. P. Singh, S. Mukherjee, N. Parzyk, G. Balakrishnan, M. R. Lees, C. D. Dewhurst, E. Babaev, A. D. Hillier, and D. M. Paul, Coexistence of type-I and type-II superconductivity signatures in ZrB_{12} probed by muon spin rotation measurements, *Phys. Rev. B* **102**, 144523 (2020).
- [24] S. Ooi, M. Tachiki, T. Konomi, T. Kubo, A. Kikuchi, S. Arisawa, H. Ito, and K. Umemori, Observation of intermediate mixed state in high-purity cavity-grade Nb by magneto-optical imaging, *Phys. Rev. B* **104**, 064504 (2021).
- [25] X. S. Brems, S. Mühlbauer, W. Y. Córdoba-Camacho, A. A. Shanenko, A. Vagov, J. A. Aguiar, and R. Cubitt, Current-induced self-organisation of mixed superconducting states, *Supercond. Sci. Technol.* **35**, 035003 (2022).
- [26] S. Datta, S. Howlader, Arushi, R. P. Singh, and G. Sheet, Anisotropic superconductivity in ZrB_{12} near the critical Bogomolnyi point, *Phys. Rev. B* **105**, 094504 (2022).
- [27] A. Vagov, A. A. Shanenko, M. V. Milošević, V. M. Axt, V. M. Vinokur, J. A. Aguiar, and F. M. Peeters, Superconductivity between standard types: Multiband versus single-band materials, *Phys. Rev. B* **93**, 174503 (2016).
- [28] A. Vagov, S. Wolf, M. D. Croitoru, and A. A. Shanenko, Universal flux patterns and their interchange in superconductors between types I and II, *Commun. Phys.* **3**, 58 (2020).
- [29] A. Vagov, T. T. Saraiva, A. A. Shanenko, A. S. Vasenko, J. Albino Aguiar, V. S. Stolyarov, and D. Roditchev, Intertype superconductivity in ferromagnetic superconductors, *Commun. Phys.* **6**, 284 (2023).
- [30] P. M. Marychev, A. A. Shanenko, A. V. Vagov, Intertype superconductivity evoked by the interplay of disorder and multiple bands, *Front. Phys.* **19**, 43205 (2024).
- [31] S. Wolf, A. Vagov, A. A. Shanenko, V. M. Axt, and J. A. Aguiar, Vortex matter stabilized by many-body interactions, *Phys. Rev. B* **96**, 144515 (2017).
- [32] W. Y. Córdoba-Camacho, A. Vagov, A. A. Shanenko, J. Albino Aguiar, A. S. Vasenko, and V. S. Stolyarov, Vortex interactions and clustering in thin superconductors, *J. Phys. Chem. Lett.* **12**, 4172 (2021).
- [33] E. B. Bogomolnyi and A. I. Vainstein, Stability of strings in gauge Abelian theory, *Sov. J. Nucl. Phys.* **23**, 588 (1976).
- [34] E. B. Bogomolnyi, The stability of classical solutions, *Sov. J. Nucl. Phys.* **24**, 449 (1976).
- [35] A. E. Jacobs, First-order transitions at H_{c1} and H_{c2} in type II superconductors, *Phys. Rev. Lett.* **26**, 629 (1971).
- [36] L. Kramer, Interaction of vortices in type II superconductors and the behavior near H_{c1} at arbitrary temperature, *Z. Phys. A* **258**, 367 (1973).
- [37] U. Klein, L. Kramer, W. Pesch, D. Rainer, and J. Rammer, Microscopic calculations of vortex structure and magnetization curves for type II superconductors, *Acta Phys. Hung.* **62**, 27 (1987).
- [38] U. Klein, Microscopic calculations on the vortex state in type II superconductors, *J. Low Temp. Phys.* **69**, 1 (1987).
- [39] P. Miranovic and K. Machida, Thermodynamics and magnetic field profiles in low- κ type-II superconductors, *Phys. Rev. B* **67**, 092506 (2003).
- [40] I. Luk'yanchuk, Theory of superconductors with κ close to $1/\sqrt{2}$, *Phys. Rev. B* **63**, 174504 (2001).
- [41] V. D. Neverov, A. Kalashnikov, A. E. Lukyanov, A. V. Krasavin, M. D. Croitoru, and A. Vagov, Fully microscopic treatment of magnetic field using Bogoliubov-de Gennes approach, *Condens. Matter* **9**, 8 (2024).
- [42] J.-X. Zhu, *Bogoliubov-de Gennes Method and Its Applications* (Springer, Berlin, 2016).
- [43] L. P. Gor'kov and T. K. Melik-Barkhudarov, Contribution to the theory of superfluidity in an imperfect Fermi gas, *Sov. Phys. JETP* **13**, 1018 (1961).
- [44] H. Heiselberg, C. J. Pethick, H. Smith, and L. Viverit, Influence of induced interactions on the superfluid transition in dilute Fermi gases, *Phys. Rev. Lett.* **85**, 2418 (2000).
- [45] <https://rscf.ru/project/23-72-30004/>